# Low-angle shear within the exposed Mânzălești diapir, Romania: salt decapitation in the Eastern Carpathians fold-and-thrust belt

Dan M. Tămaş[1], Alexandra Tămaş[1,2], Jessica Barabasch[3], Mark G. Rowan[4], Zsolt Schleder[5], Csaba Krézsek[6] and Janos L. Urai[3]

[1]*Babeș-Bolyai University, Department of Geology and Center for Integrated Geological Studies, Cluj-Napoca, Romania*

[2]*Durham University, Department of Earth Sciences, Durham, UK*

[3]*RWTH Aachen University, Tectonics and Geomechanics, Aachen, Germany*

[4]*Rowan Consulting, Inc., 850 8th St., Boulder, CO 80302, USA*

[5]*OMV Exploration & Production GmbH, Vienna, Austria*

[6]*OMV Petrom S.A., Exploration B.U., Bucharest, Romania*

## Key points

- the Mânzălești salt diapir originated as either a salt-cored anticline or a passive diapir in front of the Tarcău nappe
- foreland-directed movement of the nappe decapitated the salt body, shearing its upper portion at a shallow depth and fast strain rates
- this shear zone, exposed by uplift and erosion, forms the present-day outcrop

## ABSTRACT

In salt-detached fold-and-thrust belts, contractional modification of salt structures may include decapitation by thrusting, but examples are not well known in the subsurface and unreported in outcrop. Here we present a surface exposure of an intrasalt, sub-horizontal shear zone at the boundary between the Tarcău and Subcarpathian nappes in the Romanian

Eastern Carpathians. The Mânzălești diapir forms the largest rock salt outcrop in Europe, with unique salt-karst geomorphology. Numerous wells show that the outcrop is above deep-seated salt of a precursor salt-cored anticline or passive diapir whose base is at >3500 m. Multiscale observations using UAV-based digital outcrop models, fieldwork, and microstructure analysis show that the outcrop is characterized by sub-horizontal foliation with isoclinal folds, unlike the subvertical fabric of most Romanian diapirs. The halite is rich in clastic inclusions, with a power-law size distribution caused by tectonic reworking of originally dirty salt. Microstructures show that the halite matrix is strongly deformed by dislocation creep, forming subgrains and dynamically recrystallized grains around large porphyroclasts with piezometry indicating relatively high differential stress of around 4 MPa, at pressures sufficient to suppress dilatancy. The observations are best explained by sub-horizontal shear generated by an overriding nappe, overprinting an original coarse-grained salt fabric during decapitation of the salt body.

**Keywords:** salt tectonics, fold and thrust belt, sheared diapir, UAV photogrammetry, microstructures

## INTRODUCTION

Numerous orogenic fold-and-thrust belts involve salt, with notable examples in Arctic Canada, the Sierra Madre Oriental of Mexico, the Atlas Mts., the Pyrenees, the Alps, the Carpathians, the Zagros Mts., the Salt Ranges of Pakistan, the Kuqa Basin of China, and the Flinders Ranges of Australia (see Davis & Engelder, 1985; Letouzey et al., 1995; Hudec & Jackson, 2007; Duffy et al., 2018 for compilations and further references). In all cases, the salt layer served as an excellent décollement for salt-cored folds and salt-detached thrusts (Davis & Engelder, 1985). In some, diapirs exerted a profound influence on structural styles (e.g., Rowan & Vendeville, 2006; Callot et al., 2007). Some of these were preexisting passive diapirs that localized contractional strain (e.g., Zagros Mts.; Letouzey & Sherkati, 2004; Jahani et al., 2009, Alps; Granado et al., 2019); others developed only during the shortening. Late diapirs may initiate by salt breaking through the thin roof of an early salt-cored anticline or the thicker roof of a later fold that is thinned erosionally (Coward & Stewart, 1995), or by salt in the hanging wall of a thrust carried up to shallow levels where it can break through to the surface (Rowan, 2020). Also, salt carried up in the hanging wall of a thrust fault is also a form of diapir because the salt has a truncating relationship with younger strata in the footwall (Hudec & Jackson, 2011). This includes a late thrust that cuts one or both limbs of a precursor salt-cored anticline (break-thust fold of Willis, 1893; thrusted diapir fold of Mrazec, 1910; injection fold of Beloussov, 1959).

Whatever the timing and nature of their origin, early salt structures are subsequently modified by ongoing contractional deformation. One form of modification is decapitation, in which the upper part of a salt body or its equivalent weld is offset and transported laterally away from its deeper stem or pedestal by thrust faults. Indeed, partly or wholly decapitated diapirs have been produced in analogue and numerical models (e.g., Callot et al., 2007; Ferrer, 2012; Pichel et al., 2017; Duffy et al., 2018) and interpreted in the subsurface (e.g., Parravano et al., 2015; Snidero et al., 2019). The thrusts may emanate from within the precursor salt body itself, for example in the case of break-thrust folds, or originate away from the diapir and ramp up through the stratigraphy to intersect the salt higher up on the structure.

Developing a proper understanding of how precursor salt structures and ongoing contractional deformation interact is an important and ongoing research topic for both academia and industry. Despite their being generated in models, interpreted on seismic data, and depicted in cross sections, decapitated diapirs have not, to our knowledge, been documented in exposures in orogenic fold-and-thrust belts. Thus, this paper aims to use subsurface data, UAV-based digital outcrop models, outcrop observations, and microstructural analysis to demonstrate that the Mânzălești diapir in the Eastern Carpathians of Romania is a decapitated salt structure, whether that was a precursor passive diapir or a salt-cored anticline. We anticipate that our findings will spur others, specifically those who are taking a renewed interest in the role of salt in fold-and-thrust belts, to consider the process of diapir or fold decapitation and perhaps identify and analyze further examples.

## GEOLOGIC SETTING

### *Tectonics and stratigraphy*

The study area is located in the south of the Romanian Eastern Carpathians, in the thin-skinned part of this fold and thrust belt (Fig. 1). The Carpathians are an Alpine orogen that records the late Jurassic to middle Miocene closure of the Alpine Tethys (Săndulescu, 1988, 1984; Schmid et al., 2008; Csontos & Vörös, 2004; Mațenco, 2017; Schleder et al., 2019; Fig. 1).

The Mânzălești diapir (Fig. 2) is one of many salt outcrops located in front of the Tarcău nappe (Dumitrescu, 1948, 1952), in this case at its exposed boundary with the Subcarpathian nappe (Mrazec & Voitești, 1914; Băncilă, 1958; Fig. 2a, b). These nappes were emplaced mainly during the middle Miocene contractional event, when the Subcarpathian nappe was thrusted over the undeformed foreland (Săndulescu, 1988, 1984; Mațenco & Bertotti, 2000). The foreland deposits (Fig. 2) are represented by Sarmatian (middle Miocene) to recent clastic sedimentary rocks deposited in the Dacian Basin (see Lazarev et al., 2020, for more details).

The rocks in the Tarcău nappe are of Mesozoic to middle Miocene age, while the sequence of the Subcarpathian nappe is predominantly Eocene to mid-Miocene, although of different facies compared to the Tarcău nappe (i.e. Băncilă, 1958, Săndulescu, 1984). The number of salt formations in the Romanian Carpathians and their precise age (early or middle Miocene) is interpreted differently by different authors (i.e. Cobălcescu, 1883; Athanasiu, 1916; Mrazec & Teisseyre, 1902; Voitești, 1943; Tămaş et al., 2018; Filipescu et al., 2020). However, because this discussion is not critical for our interpretation, we use an early Miocene age for the salt in this paper.

***The Mânzălești diapir***

The Mânzălești diapir is located between the villages of Mânzălești and Lopătari (Fig. 2a), at the contact between the Tarcău and Subcarpathian nappes (Figs. 2a, b, Murgeanu et al., 1968). The western flank of the diapir is represented by the hanging wall of the Tarcău nappe and comprises early Miocene strata (Dumitrescu et al., 1970; Stoica & Gherasie, 1981; Mațenco & Bertotti, 2000; Fig. 2a, b). Immediately east of the diapir, the stratigraphy is represented by early Miocene rocks assigned to the Subcarpathian nappe (Dumitrescu et al., 1970; Stoica and Gherasie, 1981; Mațenco and Bertotti, 2000; Fig. 2b, c).

The top of the salt diapir, known as the Meledic Plateau, is capped by Quaternary fluvial sediments. The area has been the focus of multiple studies related to salt karst formation. This outcrop hosts the 6S cave, which has 3234 m of passages and is the longest salt cave in Europe and the second longest in the world (Giurgiu, 2010; Melinte-Dobrinescu et al., 2017; Ponta, 2019). The caves within the salt diapir host multiple vegetal and animal remains (i.e. a >12000-year-old molar from an Eqvus hemionus; Giurgiu, 2010). The salt is eroded quite rapidly: it is estimated that the Slănicul de Buzău river carries ~500.000 tons of dissolved halite per year (Stoica & Gherasie, 1981).

The salt is rather impure (82 vol % halite; Stoica & Gherasie, 1981; Giurgiu, 2010), even excluding the very large (decimeter- to meter-scale) inclusions (i.e. sandstones, limestones, metamorphics). The origin of the inclusions (tectonic or sedimentary) has long been debated.

They have a range of lithologies and could be derived from multiple sources, i.e. the Tarcău or older nappes or Miocene conglomerate within the Tarcău nappe (Stoica & Gherasie, 1981; Meruțiu, 1912; Dumitrescu et al., 1970; Mrazec & Teisseyre, 1902; Popescu, 1951; Olteanu, 1951; Melinte-Dobrinescu et al., 2017).

More than twenty salt and hydrocarbon exploration wells were drilled in the area. They indicate that the base of the salt is at ~3500 m (Meruțiu, 1912; Stoica & Gherasie, 1981; Mațenco & Bertotti, 2000; Fig. 2b).

## METHODS AND DATA

In this study we combine well data, satellite images and Digital Elevation Model (DEM) data with Unmanned Aerial Vehicle (UAV) photogrammetry, field observations and microstructural analysis in a multiscale analysis of internal deformation and structural evolution of the Mânzălești salt diapir.

During recent years, the use of UAV photogrammetry has become a key component of fieldwork in geoscience. Tools for interpreting 3D outcrops in Digital Outcrop Models (DOM) are emerging, and extracting structural data from outcrops that are not easy or safe to reach is now possible. Studies using UAV-based methods can much improve observations regarding both geomorphology and deformation (i.e. Weismüller et al., 2019; Mercuri et al., 2020; Fernandez et al., 2021). Field studies in outcrop and salt mines, combined with microstructural analysis, provide a scale of observation and resolution which complements 3D seismic and drill core data on geometry and allow microtectonic analysis, which provides information on rheology and deviatoric stress (i.e. Talbot & Rogers, 1980; Urai et al., 1986; Talbot, 1998; Jahani et al., 2007; Desbois et al., 2010; Schorn & Neubauer, 2014; Závada et al., 2015; Gutiérrez & Lizaga, 2016; Burliga et al., 2018; Sarkarinejad et al., 2018; Zucker et al., 2019).

A vintage 2D seismic line along the Râmnicul Sărat valley and seven exploration wells (for salt mining and hydrocarbons) were available for this study in the area of the diapir (Meruțiu, 1912; Marica, 2016; Stoica & Gherasie, 1981). The seismic line has an overall poor quality but was useful to interpret some geometries in the Miocene stratigraphy of the Subcarpathian nappe and foreland deposits to the east of the diapir. The wells were critical to better define the subsurface shape of the diapir as well as the base of the salt body. Preexisting maps, field measurements and detailed observations were used to complement the interpretation of the subsurface data. Results from analogue modelling experiments aiming to understand deformation in the Eastern Carpathian Bend Zone (Tămaș et al., 2019) provided useful structural analogues in interpreting the sub-surface data.

***Satellite data***

The satellite imagery is publicly available from ESRI. DEM data is from the European Environment Agency under the framework of the Copernicus programme (European Digital Elevation Model, version 1.1 (EU-DEM v1.1), with a pixel size of 25 m and a vertical accuracy of +/- 7 m (land.copernicus.eu).

***Unmanned aerial vehicle photogrammetry***

In an earlier UAV-based study (Urecheatu et al., 2018), we explored data acquisition and processing for the diapir outcrops. This gave a first indication of the unexpectedly shallow dip of foliation and allowed the selection of optimal parameters for the second-generation data presented in this paper. The UAV photo data were collected using a DJI Mavic Air drone with a 12 MP image sensor. A total of 1725 digital images were acquired to create the DEM, and an orthorectified image and another 2420 digital images were acquired for the nine detailed DOM.

Before image acquisition, ground control points (GCP) were defined and their locations measured. Manual flight and photograph acquisition were used for the steep faces of the outcrops from altitudes ranging from 50 m to 150 m (Fig. 3). The photographs of the sediment-covered flat top of the diapir were taken using both manual flight paths and automated flight paths as two orthogonal flight grids. For the automated data acquisition, we used Pix4Dcapture. When flying the manual flight paths, we aimed to achieve a similar photograph overlap as with the automated acquisition.

For the creation of the DOM, DEM and orthorectified models, we used Agisoft Metashape Professional (v.1.6.2). The first step in the process aligns the photographs, generating a sparse point cloud (Fig. 3). The next step was the generation of the dense point cloud. We then generated both the DEM and the mesh from the dense point cloud, which we later textured (Fig. 3). The position match between the UAV-based orthomosaic and satellite imagery is very good, thus we have high confidence in the orientation and position of the DOM.

***Structural data extraction***

The DEM and orthomosaic data were imported in QGIS (QGIS v. 3.14, 2020), used to extract boundaries of the salt outcrops and map larger inclusions in the salt, lineations and the size and geometries of the valleys and sinkholes. The 3D textured meshes (DOM) together with the dense point cloud data were imported into Virtual Reality Geological Studio (VRGS v.2.52) software (Hodgetts, 2010) with the scope of interpreting them and extracting the orientation of structural features. We measured the orientation of salt foliation, shear zones and fold axial planes. Orientation data were processed in Stereonet (Allmendinger et al., 2013; Cardozo & Allmendinger, 2013) and Structural Geology to Post Script (SG2PS; Sasvári & Baharev, 2014).

### ***Ground-based fieldwork***

Field observations provided information on lithology, orientation of bedding (non-salt units) and foliation in salt and on the structure of salt crusts covering much of the outcrop (Fig. 4). Where accessible, dip and azimuth measurement were taken using both a Freiberg geological compass and FieldMove on an iPad. This helped ground-truth the UAV-DOM observations. We note here that access to outcropping rock salt which is not covered by salt crust is limited, because access to the steep outcrop faces is dangerous. We collected one unoriented sample which looked representative to other outcrops which were visible but not accessible, from the south-eastern area of the diapir (see Fig. 5). Another sample we studied was received from a fellow researcher (Dan Jipa) for microstructural study.

### ***Microstructural analysis***

Samples for microstructural analysis were cut in a dry laboratory with a diamond saw cooled by a small amount of slightly undersaturated salt brine to reduce damage. Gamma-irradiation was done at a temperature of 100°C to a total dose of about 4 MGy, at a DFG-supported, purpose-built irradiation facility at the Research Reactor FRM II in Munich, Germany. Thin sections were polished to a thickness of approximately 1 mm and then chemically polished and etched using the technique described in Urai et al. (1987).

The thin sections were imaged in plane polarized (ppl) and reflected light using a Zeiss optical microscope. Halite grain and subgrain boundaries were manually traced with a touchpen and tablet and analyzed with Fiji (Schindelin et al. 2012) for subgrain size piezometry (Schleder & Urai 2005). Thereby the grain size was calculated as equivalent circular diameters by only taking halite grains into account. Non-halite inclusions of one hand specimen were peeled onto acrylic foil, scanned and image processed with Fiji

(Schindelin et al. 2012). This contributed to an accurate mapping of non-halite inclusions by the utilization of Fiji image thresholding. For X-ray diffraction (XRD) analysis of inclusions, a hand specimen was dissolved in water, and the insoluble residue was hand-picked into three particle classes based on colour (black, beige and greenish). Qualitative and quantitative XRD measurements were then performed on a Bruker D8 equipped with a graphite monochromator and a scintillation counter. Scans were measured with Cu-kα radiation.

## RESULTS

### *Geomorphology*

The extent of salt close to the surface is about 2.7 km by 1.3 km, with karstified halite cut by hypersaline streams (Fig. 5). The maximum elevation difference between the lowest point in the riverbed crossing the salt diapir and the highest point of the diapir is 198.5 m. The highest point (613 m) is located in the east-central part of the salt outcrop. Much of the flat top of the salt is covered (Figs. 5-8) by thin quaternary strata and soil, grass, bushes and trees. Salt is only outcropping in steep exposures. When exposed, the salt is usually white to light-grey and the surrounding stratigraphy is pale yellow-brown. Combining our data with geological maps and other published data, we estimated the area of salt which is covered by thin quaternary strata (dashed red line in Fig. 5).

### *UAV-based models*

Four of the nine high-resolution digital outcrop models provided sufficient outcrop quality to allow interpretation and analysis of structures; three of these are described in the paper (Fig. 5). The models have been classified as good (green color in Fig. 5), moderate (yellow color in Fig. 5) or poor quality (orange color in Fig. 5) based on the exposure quality, amount of debris cover and model generation quality.

The models presented expose the foliation and other structures of the salt. Foliation orientation measurements were possible because the deep gullies in the outcrop faces provide two apparent dip measurements (Fig. 5). As will be discussed below, foliation in the salt is generally gently dipping, with some variations between outcrops.

***Digital Outcrop Model 1***

This DOM (shown in Fig. 6) is located in the northern part of the Mânzălești salt diapir (Fig. 5). This is the only area in the north where salt layering is visible in DOM. The model is 170 m long and 85 m high and has an east-west orientation (Figs. 5, 6). The exposure and model quality are relatively good, with some areas covered by recrystallized salt crusts and debris (Fig. 6). The salt foliation (n = 30) has an average dip of 23° to the SW (Fig. 6d). Sandstone interlayered with the salt are shown in detail in (Fig. 6c).

***Digital Outcrop Model 2***

The DOM (shown in Fig. 7) is from the south-western edge of the study area, located along the main road between Mânzălești and Lopătari (Fig. 5). The model is 200 m long and 47 m high and has a WSW–ENE orientation (Figs. 5, 7a, c). The exposure and model quality are relatively good, locally covered by recrystallized salt crusts and debris. Several sinkholes can be identified in the model (Fig. 7a, c), ranging from 2-40 m in width and with depths up to 23 m.

Folds in the salt could not be identified in this outcrop. The salt foliation orientations are the steepest in this area, 53° to the NE (Fig. 7b, e)), locally cross-cut by white, subparallel, low-dipping bands (17° NW; Fig. 7b) whose origin is discussed below. In the western edge of the model, near-vertical (82° WSW; Fig. 7a, d, f) rocks of the Tarcău nappe are exposed and truncated by Quaternary fluvial sediments (Fig. 7d).

### *Digital Outcrop Model 3*

The DOM (Fig. 8) is located near the southern edge of the study area, along the main road between Mânzălești and Lopătari (Fig. 5). It is west-east oriented with a length of 300 m and a height of 90 m (Fig. 8). The good exposure quality of the 3-D model enabled the extraction of 172 foliation measurements, with an average dip of 20° to the NW (Fig. 8d). We mapped multiple isoclinal folds of the foliation defined by different shades of grey banding (caused by varying amounts and types of inclusions), which are locally slightly anastomosing, forming tectonic lenses (Figs. 8a, c). The foliation is locally cross-cut by sub horizontal white bands (8° NE; Figs. 8a, b).

The inclusion-rich halite is locally exposed in outcrops at the base of the DOM, while in other parts it is covered by a precipitated layer of fine-grained porous halite that mimics the colour of the underlying salt. The exposed halite contains inclusions in a halite matrix consisting of cm-size halite porphyroclasts surrounded by finer-grained halite (Figs. 4c, d, 9). The non-halite inclusions have a wide range in size and show no preferred orientation.

### *Results of microstructural analysis*

Both samples (Fig. 9a, c) are rich in non-halite inclusions (14 wt %, Fig. 9a). Additionally, a sample from the specimen shown in 9a has been gamma irradiated to allow for decoration of halite microstructures (Fig. 9b). Embedded in a halite matrix around the elongate halite porphyroclasts (Fig. 9d).. XRD analysis of three particle classes in the insoluble residue shows beige sandstone, greenschist, and volcanic rock. Inclusions have a power-law distribution of grain sizes (Fig. 9c) and locally have fibrous strain shadows (Fig. 9f).

The halite matrix has a characteristic dynamically recrystallized microstructure with grains of about 1.5 mm, which are slightly elongated parallel to the foliation and have irregular, amoeboid shapes. Halite fibres are locally present in boudin necks between fragmented inclusions (Fig. 9f). Gamma irradiation developed a blue colour in part of the halite grains. Some of these show a finely striped blue pattern in-between non-halite inclusions (Fig. 9b, e) indicating solution-precipitation processes. Most halite grains (including the porphyroclasts) are rich in subgrains with an average size of 52 µm (n=520). Locally, halite grains are subgrain-free and have 120° grain boundaries (Fig. 9g). Using subgrain size piezometry (Schleder & Urai, 2005), this corresponds to a relatively high differential stress of about 3.5 MPa. Recrystallized grainsize piezometry (Ter Heege et al., 2005) indicates a differential stress of about 4 MPa. High-angle grain boundaries in halite are rich in fluid inclusions and smaller non-halite particles are often present at grain boundaries and triple junctions.

***Cross-sectional geometry***

The cross-sectional geometry (Fig. 10) is constrained by a combination of the surface geology (stratigraphic boundaries, dip/azimuth of the layers, structural features) and subsurface well and seismic data. The maximum distance the well data have been projected is ~1 km. The data show that the diapir is roughly 3,500 m tall and leans to the east, with a 45º dipping western flank and a slightly steeper overhanging eastern flank.

Flanking lower Miocene strata to the west, belonging to the Tarcău Nappe, are steeply dipping (82/245) in the proximity of the salt and shallow dipping (18/234) about 200 m west of the diapir, with seismic reflections dipping on average 45º to the west, parallel to the underlying top salt (Figs. 2b, 10). Overall, they are part of a highly internally deformed major lower Miocene synform.

On the eastern flank of the diapir, the contact of the salt with adjacent layers is not visible, being covered by Quaternary deposits, but regional maps show Subcarpathian units to the east of the diapir (Fig. 2). About 500 m east of the salt edge, lower Miocene strata are exposed and dip steeply to the east. They become highly folded and thrusted, with mid-Miocene deposits in the hinges of small-scale synclines. Underlying seismic reflections suggest the presence of several thrust imbricates. This stratigraphy is buried to the east beneath the foreland deposits.

## DISCUSSION

### *Nature of the Mânzălești salt outcrop*

The Mânzălești diapir is the largest rock salt outcrop in Europe, described by many authors. However, its structure and origin were not clear, perhaps due to difficulties of access (unstable and dangerous, steep halite faces) and lack of microtectonic investigations. Using our high-resolution UAV-models and microstructural data allows for the first time a detailed structural analysis. In the discussion below, we consider four possible interpretations for the Mânzălești outcrop: (i) original subhorizontal layering of inclusion-rich depositional salt layers, (ii) eroded top of a long-lived passive diapir, (iii) salt glacier emplaced by lateral flow at the surface, and (iv) the sheared top of a decapitated salt structure.

The origin of non-halite inclusions in some salt bodies in Romania has a long history of debate because they have aspects compatible with either sedimentary or tectonic melanges. Discrete layers of mixed halite and siliciclastics exist in the spectacular domal salt mine exposures in Romania (e.g., Ocnele Mari, Târgu Ocna, Slănic Prahova, Cacica), and in our samples, original halite porphyroclasts contain clastic inclusions. Both observations suggest a depositional origin, but the isoclinal folds together with the subhorizontal, gently anastamosing salt foliation in halite with large porphyroclasts surrounded by small recrystallized grains indicates intense subhorizontal shear overprinting primary layering and/or diapiric foliation within the salt. Thus we reject hypothesis (i): in our interpretation, the inclusions most likely formed as debris flows shed into the depositional evaporite basin during orogenic uplift (similar to what is observed in the Polish and Ukrainian Carpathians; Peryt & Kovalevich, 1997; Ślączka & Kolasa, 1997), with the consequent interbedded halite and non-halite layers subsequently sheared during the superimposed deformation.

The fabric in the Mânzălești diapir contrasts strongly with the typical "domal" salt fabric observed in other Romanian diapirs. These are characterized by vertical to steeply-dipping, folded layers with larger, more equisized recrystallized grains deformed at lower differential stress. In our samples, microstructures show that halite was deformed by dislocation creep and water-assisted dynamic recrystallization under relatively high differential stresses of about 4 MPa, with solution-precipitation creep and fragmentation of the inclusions during deformation (see also Leitner et al., 2011). We interpret the gamma decorated halite stripes to have formed during solution-precipitation creep, between non-halite inclusions. The large porphyroclasts are interpreted as the remnants of the original halite fabric (Schleder & Urai 2005, 2007; Závada et al., 2015). Thus, the subhorizontal fabric and high differential stress lead us to reject the interpretation in which the Mânzălești outcrop is the eroded top of a passive diapir.

Salt glaciers are characterized by fine-grained salt deformed at very low differential stress by dominantly solution-precipitation creep (Schleder & Urai, 2007; Desbois et al., 2010), with porphyroclasts rich in subgrains inherited from the rise of salt in the cold diapiric stem. Our microstructural observations (recrystallized grains contain abundant subgrains) and calculated differential stress levels are also incompatible with this, and thus we conclude that the surface outcrop at Mânzălești is not a salt glacier.

After combining the outcrop and microstructural analyses, our preferred explanation is that the Mânzălești exposure represents a low-angle tectonic shear zone. Given the depth of salt proven by wells and the location of the diapir at the boundary between the Tarcău and

Subcarpathian nappes (Fig. 10), along with the large displacement of the Tarcău Nappe (REFS), we suggest that the intense shear records decapitation of a large salt structure by the foreland-directed movement of the Tarcău nappe. This happened at a shallow depth and fast strain rate to generate the relatively high differential stress during dominantly dislocation creep and water-assisted dynamic recrystallization with solution-deposition creep, but at sufficient depth to supress dilatancy (500 m is a reasonable estimate; see Urai et al., 2008).

***Origin of the Mânzălești diapir***

If the Mânzălești outcrop records tectonic shear during decapitation, the question remains what kind of underlying structure has been modified. Decapitated salt structures may take several forms. First, after a passive diapir is squeezed shut, forming a secondary salt weld, further shortening leads to a thrust emerging from the diapir pedestal and offsetting the weld from its root (Fig. 11a). Second, decapitation may occur slightly higher on the diapir stem during rift-basin inversion, where thrust faults ramping up over basement steps may intersect diapirs located in the footwalls of the basement faults (Fig. 11b). Third, a thrust fault may break out of a salt-cored detachment fold, thereby generating a diapir (again, break-thrust fold, thrusted diapir fold, or injection fold), shearing the salt, and ultimately translating the upper portion completely off its base (Fig. 11c). Fourth and fifth, a shallow nappe may intersect the upper part of a passive diapir (Fig. 11d) or a salt-cored anticline (Fig. 11e). Some of these styles have been produced in analogue models or interpreted in the subsurface (e.g., Callot et al., 2007, 2012; Ferrer, 2012; Parravano et al., 2015; Pichel et al., 2017; Duffy et al., 2018; Snidero et al., 2019; Santolaria et al., 2021). The example in Fig. 11f shows another variation, with one flanking minibasin of a passive diapir elevated and thrust over the other minibasin in a stage of incipient decapitation.

The intersection of the Tarcău Nappe front and the Mânzălești diapir strongly suggests that we have one of the scenarios in Fig. 11d or e. Thus, the data shown in Fig. 10 are used to generate two alternative cross sections showing either a deep salt-cored anticline or a deep passive diapir. In Fig. 12a, a truncated syncline of lower Miocene is inferred beneath the Tarcău thrust plane on the western flank of the diapir, and strata concordant to the salt edge are also indicated at the deeper levels of the eastern flank. In contrast, Fig. 12b shows lower Miocene strata truncated on both flanks. Although we have no data at Mânzălești to allow us to distinguish between these two options, we favour the salt-cored anticline interpretation (Fig. 12a). This structural style, also suggested by previous workers (i.e. Ştefãnescu et al., 1984; Mațenco and Bertotti, 2000; Schleder et al., 2019), is compatible with seismic data and existing boreholes along strike to the north and south. A seismic profile (Fig. 12a, inset; Schleder et al., 2019) shows a salt-cored anticline at the lower Miocene level truncated by a prominent unconformity with more gently dipping upper Miocene strata above, on either side of a thin vertical sliver of salt (constrained by wells). If a thrust fault intersected this geometry beneath the unconformity, the result would be a decapitated salt-cored anticline (Figs. 11e, 12a); if it intersected above the unconformity, it would be a decapitated passive diapir (Figs. 11d, 12b). The existence of lower Miocene rocks preserved on the eastern side of the Mânzălești diapir supports our favored interpretation of a decapitated salt-cored anticline.

Taking an average displacement rate on the frontal Tarcău thrust of 2 cm/year (Roure et al., 1993; Schleder et al., 2019) and a shear zone of 100 m thickness, the computed shear strain rate is $5x10^{-12}$ $s^{-1}$. If the original shear zone, including portions removed by erosion, was thicker, then the strain rate was lower. Combining this with the independently obtained estimate of the differential stress of 4 MPa, we get an estimate of the rheology of the shear zone in reasonable agreement with the constitutive equation for halite rocks deforming by equal amounts of dislocation creep and solution-precipitation creep (cf. fig. 5.2.5 of Urai et al., 2008; ter Heege et al., 2005).

Finally, we interpret the near-horizontal surfaces of white salt, sometimes cross-cutting the salt foliation, as dilatant shear zones. Although we have not been able to sample and analyse them due to inaccessibility, they likely formed during the final stages of deformation at low confining pressures close to the surface, with the colour modified by fluid flow (e.g., Urai et al., 2008; Davison, 2009). This presumably occurred during uplift and erosional unroofing of the diapir during the latest stages of nappe advance.

## CONCLUSIONS

We integrated UAV-based digital outcrop models, outcrop observations, microstructural analysis and subsurface data to gain new insights into the Mânzălești diapir located in the Eastern Carpathians of Romania. The results of our study show:

- The extent of the salt at or just beneath the surface is about 2.7 km by 1.3 km wide, with about 200 m of relief. In the subsurface, the diapir extends downward for about 3.5 km, demonstrating a deep-rooted salt body.
- In outcrop, especially in steep faces, the halite is locally exposed. It presents solution grooves (rillenkarren), while in other parts it is covered by a precipitated layer of fine-grained porous halite that mimics the colour of the underlying salt.
- UAV-based digital outcrop models enabled the measurement of generally low-dipping (20-34°) salt foliation, with a higher average in the SW edge of the salt dome (53°). Isoclinal folds and low-dipping shear zones have also been identified.
- The exposed salt is rich in impurities, ranging from micrometer to m-scale fragments of various lithologies (sandstones, limestones, green schists, volcanics). These are

interpreted as originating as sedimentary layers interbedded with the halite, and later disrupted by deformation.

- The impurities are hosted in a matrix of halite consisting of cm-size porphyroclasts surrounded by finer-grained halite.
- Microstructures show that halite was deformed by dislocation creep and water-assisted dynamic recrystallization under relatively high differential stresses of about 4 MPa, with solution-precipitation creep and fragmentation of the non-halite inclusions during deformation.

The observed fabric and microstructural analysis, combined with subsurface data and the location of the outcrop at the frontal edge of the Tarcău nappe, document a low-angle shear zone that records decapitation of a deep-seated salt structure during advance of the nappe. Although the deep salt structure might have been a passive diapir, we interpret it instead as having originated as a salt-cored anticline based on other observed structures along strike. Foreland-directed movement of the nappe sheared the top of the fold during decapitation. The deformation happened at a shallow depth and fast strain rates, as demonstrated by the microstructural analysis.

**ACKNOWLEDGEMENTS**

Relu D. Roban and Dan Jipa are thanked for insightful discussions. We thank Dan Jipa for donating one of the halite samples for this study. XRD analysis was performed by Nicolai Thüns. Schlumberger and M. El Toukhy kindly provided the seismic data in Fig. 11f. DMT acknowledges financial support from Babeș-Bolyai University, through the Young Researcher Grant no. 35275/18.11.2020.

## DATA AVAILABILITY

The three digital outcrop models as well as the overview 3D model have been uploaded to Pangaea repository and will soon be available.

## REFERENCES

Allmendinger, R. W., Cardozo, N. C., & Fisher, D. (2013). *Structural Geology Algorithms: Vectors & Tensors*. Cambridge, UK: Cambridge University Press.

Athanasiu, S. (1916). Discuționea asupra vârstei formațiunei salifere din România. *Dări de Seamă, Institutul Geologic al României*, 5, 22–32.

Băncilă, I. (1958). *Geologia Carpaților Orientali*. Bucharest, Romania: Editura Tehnică.

Beloussov, V. V. (1959). Types of folding and their origin. *International Geology Review*, 1(2), 1-21. https://doi.org/10.1080/00206815909473393

Burliga, S., Krzywiec, P., Dąbroś, K., Przybyło, J., Włodarczyk, E., Źróbek, M., & Słotwiński, M. (2018). Salt tectonics in front of the Outer Carpathian thrust wedge in the Wieliczka area (S Poland) and its exposure in the underground salt mine. *Geology, Geophysics & Environment*, 44(1), 71. https://doi.org/10.7494/geol.2018.44.1.71

Callot, J.-P., Jahani, S., & Letouzey, J. (2007). The role of preexisting diapirs in fold and thrust best development. In O. Lacombe, F. Roure, J. Lavé, J. Vergés, (Eds.), *Thrust Belts and Foreland Basins* (pp. 309-325). Berlin: Springer. https://doi.org/10.1007/978-3-540-69426-7_16

Cardozo, N., & Allmendinger, R. W. (2013) Spherical projections with OSXStereonet: *Computers & Geosciences*, 51, 193-205. https://doi.org/10.1016/j.cageo.2012.07.021

Cobălcescu, G. (1883). *Studii geologice și paleontologice asupra unor tĕràmuri terțiare din unile părți ale Romăniei: Memoriile Geologice ale Scolei Militare din Iasi*. Bucharest, Romania: Stabilimentul grafic Socecu & Teclu.

Coward, M. P., & Stewart, S. (1995). Salt-influenced structures in the Mesozoic-Tertiary cover of the southern North Sea, U.K. In M. P. A. Jackson, D. G. Roberts, S. Snelson (Eds.), *Salt tectonics: a global perspective* (AAPG Memoir 65, pp. 229-250), AAPG. https://doi.org/10.1306/M65604C10

Csontos, L. & Vörös, A. (2004). Mesozoic plate tectonic reconstruction of the Carpathian region. *Palaeogeography, Palaeoclimatology, Palaeoecology*, 210, 1–56. https://doi.org/10.1016/j.palaeo.2004.02.033

Davis, D. M., & Engelder, T. (1985). The role of salt in fold-and-thrust belts. *Tectonophysics*, 119, 67-88. https://doi.org/10.1016/0040-1951(85)90033-2

Davison, I. (2009). Faulting and fluid flow through salt. *Journal of the Geological Society*, 166(2), 205–216. https://doi.org/10.1144/0016-76492008-064

Desbois, G., Závada, P., Schleder, Z., & Urai, J. L. (2010) Deformation and recrystallization mechanisms in actively extruding salt fountain: Microstructural evidence for a switch in deformation mechanisms with increased availability of meteoric water and decreased grain size (Qum Kuh, Central Iran). *Journal of Structural Geology*, 32(4), 580-594. https://doi.org/10.1016/j.jsg.2010.03.005

Duffy, O. B., Dooley, T. P., Hudec, M. R., Jackson, M. P. A., Fernandez, N., Jackson, C. A.-L., & Soto, J. I. (2018). Structural evolution of salt-influenced fold-and-thrust belts: a synthesis and new insights from basins containing isolated salt diapirs. *Journal of Structural Geology*, 114, 206-221. https://doi.org/10.1016/j.jsg.2018.06.024

Dumitrescu, I. (1948). La Nappe du Gres de Tarcău, la zone marginale et la zone neogene, entre Casin et Putna: Comptes Rendus deo Seances. *Institut Geologique de Roumanie*, 29, 84–105.

Dumitrescu, I. (1952). Etude Geologique de la region entre l'Oituz et la Coza. *Anuarul Institutului Geologic al Romaniei*, 14, 195–218.

Dumitrescu, I., Săndulescu, M., & Bandrabur, T. (1970). *Geological Map of Romania (sheet 29-Covasna, scale 1:200000)*. Bucharest, Romania: Geological Institute of Romania, explanatory text, 80 p.

Fernandez, O., Habermüller, M., & Grasemann, B. (2021). Hooked on salt: Rethinking Alpine tectonics in Hallstatt (Eastern Alps, Austria). *Geology*, 49(3), 325-329. https://doi.org/10.1130/G47981.1

Ferrer, J. O. (2012). Salt Tectonics in the Parentis Basin (Eastern Bay of Biscay): Origin and Kinematics of Salt Structures in a Hyperextended Margin Affected by Subsequent Contractional Deformation (Doctoral dissertation). Barcelona, Spain, University of Barcelona.

Filipescu, S., Tămaș D. M., Bercea R., Tămaș A., Bălc, R., Țabără, D., et al. (2020). The biostratigraphic reevaluation of the lower to middle Miocene formations from the Eastern Carpathians: a case study related to the oil fields of the Diapir Fold Zone, Romania. *Geological Quarterly*, 64(3), 781–800. https://doi.org/10.7306/gq.1554

Giurgiu, I. (2010). Cea mai mare peșteră în sare din România. *Natura României*, 3, 1-234.

Hodgetts, D. (2010). *Collection, processing, interpretation and modelling of digital outcrop data using VRGS: An integrated approach to outcrop modelling*. Paper presented at 72nd EAGE Conference and Exhibition-Workshops and Fieldtrips (pp. cp-162).

Granado, P., Roca, E., Strauss, P., Pelz, K., Muñoz, J.A. (2019). Structural styles in fold-and-thrust belts involving early salt structures: The Northern Calcareous Alps (Austria). *Geology*, 47 (1), 51–54. https://doi.org/10.1130/G45281.1

Hudec, M. R., & Jackson, M. P. A. (2007). Terra infirma: understanding salt tectonics. *Earth-Science Reviews*, 82, 1-28. https://doi.org/10.1016/j.earscirev.2007.01.001.

Hudec, M. R., & Jackson, M. P. A. (2011). *The Salt Mine: a Digital Atlas of Salt Tectonics*. Bureau of Economic Geology, Udden Book Series No. 5, AAPG Memoir 99. Austin, Texas, The University of Texas at Austin, 305 p.

Jackson, M. P. A., & Hudec, M. R. (2017). *Salt Tectonics – Principles and Practice*. Cambridge, UK: Cambridge University Press. https://doi.org/10.1017/9781139003988

Jahani, S., Callot, J.-P., Letouzey, J., & Frizon de Lamotte, D. (2009). The eastern termination of the Zagros Fold-and-Thrust Belt, Iran: structures, evolution, and relationships between salt plugs, folding, and faulting. *Tectonics*, 28, TC6004. https://doi.org/10.1029/2008TC002418

Lazarev, S., de Leeuw, A., Stoica, M., Mandic, O., van Baak, C. G. C., Vasiliev, I., & Krijgsman, W. (2020). From Khersonian drying to Pontian flooding: late Miocene stratigraphy and palaeoenvironmental evolution of the Dacian Basin (Eastern Paratethys). *Global and Planetary Change*, 192, 103224. https://doi.org/10.1016/j.gloplacha.2020.103224

Leitner, C., Neubauer, F., Urai, J. L., & Schoenherr, J. (2011). Structure and evolution of a rocksalt-mudrock-tectonite: The Haselgebirge in the Northern Calcareous Alps. *Journal of Structural Geology*, 33(5), 970-984. https://doi.org/10.1016/j.jsg.2011.02.008

Letouzey, J., Colletta, B., Vially, R., & Chermette, J. C. (1995). Evolution of salt-related structures in compressional settings. In M. P. A. Jackson, D. G. Roberts, S. Snelson (Eds.), *Salt tectonics: a global perspective* (AAPG Memoir 65, pp. 41-60), AAPG. https://doi.org/10.1306/M65604C3

Marica, I. S. (2016). Aplicaţii ale măsurătorilor geofizice în studiul masivelor de sare din România - Zona Cutelor Diapire (Doctoral dissertation). Bucharest, Romania, Bucharest University.

Mațenco, L., & Bertotti, G. (2000). Tertiary tectonic evolution of the external East Carpathians (Romania). *Tectonophysics*, 316, 255–286. https://doi.org/10.1016/S0040-1951(99)00261-9

Mațenco, L. (2017). Tectonics and exhumation of the Romanian Carpathians: Inferences from kinematic and thermochronological studies. In M. Radoane, A. Vespremeanu-Stroe (Eds.), *Landform Dynamics and Evolution in Romania* (pp. 15-56), Springer Geography. https://doi.org/10.1007/978-3-319-32589-7_2

Melinte-Dobrinescu, M. C., Brustur, T., Jipa, D., Macaleţ, R., Ion, G., Ion, E., et al. (2017). The Geological and Palaeontological Heritage of the Buzău Land Geopark (Carpathians, Romania). *Geoheritage*, 9, 225–236. https://doi.org/10.1007/s12371-016-0202-3

Mercuri, M., McCaffrey, K.J.W., Smeraglia, L., Mazzanti, P., Collettini, C., & Carminati, E. (2020). Complex geometry and kinematics of subsidiary faults within a carbonate-hosted relay ramp. *Journal of Structural Geology*, 130, 103915. https://doi.org/10.1016/j.jsg.2019.103915

Meruțiu, V. (1912). *Contribuțiune la studiul masivelor de sare din România*. Bucharest, Romania: Stabilimentul de arte grafice Albert Baer.

Mrazec, L. (1910). Über die Bildung der rumänischen Petroleumlagerstätten. *Third International Petroleum Conference: Compte Rendu*, 2, 80-134.

Mrazec, L., & Teisseyre, W. (1902). Privire geologică asupra formaţiunilor salifere şi zăcămintelor de sare din România. *Monitorul Petrolului Român*, 3, 1–55.

Mrazec, L. & Voitești, I. P. (1914). Contributions a la connaissance des nappes du Flysch Carpatique en Roumanie. *Anuarul Institutului Geologic al Romaniei*, 5, 495–527.

Murgeanu, G., Dumitrescu, I., Săndulescu, M., Bandrabur, T., & Săndulescu, J. (1968) *Geological Map of Romania (sheet 29-Covasna, scale 1:200000)*. Bucharest, Romania: Geological Institute of Romania.

Olteanu, F. (1951). Observații asupra 'breciei sării', cu masive de sare din regiunea mio-pliocenă dintre R. Teleajenului și P. Bălăneasa (cu privire specială pentru regiunea Pietraru-Buzău). *Dări de Seamă, Institutul geologic al României*, 32, 12-18.

Parravano, V., Teixell, A., & Mora, A. (2015). Influence of salt in the tectonic development of the frontal thrust belt of the eastern Cordillera (Guatiquía area, Colombian Andes). *Interpretation*, 3(4), 17-27. https://doi.org/10.1190/INT-2015-0011.1

Peryt, T. M., & Kovalevich, V. M. (1997). Association of redeposited salt breccias and potash evaporites in the Lower Miocene of Stebnyk (Carpathian foredeep, West Ukraine): *Journal of Sedimentary Research*, 67, 913–922. https://doi.org/10.1306/D4268676-2B26-11D7-8648000102C1865D

Pichel, L. M., Finch, E., Huuse, M., & Redfern, J. (2017). The influence of shortening and sedimentation on rejuvanation of salt diapirs: a new discrete-element modelling approach. *Journal of Structural Geology*, 104, 61-79. https://doi.org/10.1016/j.jsg.2017.09.016

Ponta, G. M. L. (2019). Eastern Subcarpathians Bend: Salt Karst: Meledic Plateau and Slănic Prahova. In G. M. L. Ponta, B. P. Onac (Eds.), *Cave and Karst Systems of Romania, Cave and Karst Systems of the World* (pp. 451–454), Springer International Publishing. https://doi.org/10.1007/978-3-319-90747-5_51

Popescu, G. (1951). Observațiuni asupra ‘breciei sării’ și a unor masive de sare din zona paleogenă-miocenă a jud. Prahova. *Dări de Seama, Institutul geologic al României*, 32, 3-12.

QGIS Development Team (2020). *QGIS Geographic Information System*. Open Source Geospatial Foundation Project. http://qgis.osgeo.org

Roure, F., Roca, E., & Sassi, W. (1993). The Neogene evolution of the outer Carpathian flysch units (Poland, Ukraine and Romania): kinematics of a foreland/fold-and-thrust belt system. *Sedimentary Geology*, 86, 177–201. https://doi.org/10.1016/0037-0738(93)90139-V

Rowan, M. G. (2020). Salt- and shale-detached gravity-driven failure of continental margins. In: N. Scarselli, J. Adam, D. Chiarella, D. G. Roberts, & A. W. Bally (Eds.), *Regional Geology and Tectonics, Vol. 1: Principles of Geologic Analysis (2nd Edition)*, 205-234.

Rowan, M. G., & Vendeville, B. C. (2006). Foldbelts with early salt withdrawal and diapirism: physical model and examples from the northern Gulf of Mexico and the Flinders Ranges, Australia. *Marine and Petroleum Geology*, 23, 871-891. https://doi.org/10.1016/j.marpetgeo.2006.08.003

Săndulescu, M. (1984). *Geotectonica României*. Bucharest, Romania: Editura Tehnică.

Săndulescu, M. (1988). Cenozoic Tectonic History of the Carpathians. In: L. H. Royden, F. Horváth (Eds.), *The Pannonian Basin: A Study in Basin Evolution* (AAPG Memoir 45, pp. 17–25), AAPG. https://doi.org/10.1306/M45474C2

Santolaria, P., Ferrer, O., Rowan, M. G., Snidero, M., Carrera, N., Granado, P., Muñoz, J. A., Roca, E., Schneider, C. L., Piña, A., & Zamora, G. (2021). Influence of preexisting salt diapirs during thrust wedge evolution and secondary welding: insights from analog modeling. *Marine and Petroleum Geology* (in press).

Sarkarinejad, K., Sarshar, M. A., & Adineh, S. (2018). Structural, micro-structural and kinematic analyses of channel flow in the Karmostaj salt diapir in the Zagros foreland folded belt, Fars province, Iran. *Journal of Structural Geology*, 107, 109–131. https://doi.org/10.1016/j.jsg.2017.12.005

Sasvári, Á., & Baharev, A. (2014). SG2PS (structural geology to postscript converter)–A graphical solution for brittle structural data evaluation and paleostress calculation. *Computers & Geosciences*, 66, 81-93. https://doi.org/10.1016/j.cageo.2013.12.010

Schindelin, J., Arganda-Carreras, I., Frise, E., Kaynig, V., Longair, M., Pietzsch T., et al. (2012). Fiji: an open-source platform for biological-image analysis. *Nature methods*, 9(7), 676-682. https://doi.org/10.1038/nmeth.2019

Schleder, Z., & Urai, J. L. (2005). Microstructural evolution of deformation- modified primary Halite from Hengelo, the Netherlands. *International Journal of Earth Sciences (Geol Rundsch)*, 94(5-6), 941-956. https://doi.org/10.1007/s00531-005-0503-2

Schleder, Z., & Urai, J. L. (2007). Deformation and recrystallization mechanisms in Mylonitic shear zones in naturally deformed extrusive Eocene-Oligocene rocksalt from Eyvanekey Plateau and Garmsar Hills (Central Iran). *Journal of Structural Geology*, 29(2), 241-255. https://doi.org/10.1016/j.jsg.2006.08.014

Schleder, Z., Tămaş, D. M., Krézsek, C., Arnberger, K., & Tulucan, A. (2019). Salt tectonics in the Bend Zone segment of the Carpathian fold and thrust belt, Romania: *International Journal of Earth Sciences (Geol Rundsch)*, 108, 1595–1614. https://doi.org/10.1007/s00531-019-01721-x

Schmid, S. M., Bernoulli, D., Fügenschuh, B., Maţenco, L., Schefer, S., Schuster, R., et al. (2008). The Alpine-Carpathian-Dinaridic orogenic system: correlation and evolution of tectonic units. *Swiss Journal of Geosciences*, 101, 139–183. https://doi.org/10.1007/s00015-008-1247-3

Schorn, A., & Neubauer, F. (2014). The structure of the Hallstatt evaporite body (Northern Calcareous Alps, Austria): A compressive diapir superposed by strike-slip shear?. *Journal of Structural Geology*, 60, 70–84. https://doi.org/10.1016/j.jsg.2013.12.008

Sherkati, S., & Letouzey, J. (2004). Variation of structural style and basin evolution in the central Zagros (Izeh zone and Dezful Embayment), Iran. *Marine and Petroleum Geology*, 21, 535-554. https://doi.org/10.1016/j.marpetgeo.2004.01.007

Ślączka, A., & Kolasa, K. (1997). Resedimented salt in the Northern Carpathians Foredeep (Wieliczka, Poland). *Slovak Geological Magazine*, 3, 135-155.

Snidero, M., Muñoz, J.A., Carrera, N., Butillé, M., Mencos, J., Motamedi, H., et al. (2019). Temporal evolution of the Darmadan salt diapir, eastern Fars region, Iran. *Tectonophysics*, 766, 115-130. https://doi.org/10.1016/j.tecto.2019.06.006

Ştefănescu, M. et al. (1984). Elaborarea profilelor, scara 1:200.000 pentru completarea imaginii geologice a teritoriului R.S. România. Secțiunea geologica A-16, *Institutul de Geologie și Geofizică*, Bucharest, Romania.

Stoica, C., & Gherasie, I. (1981). *Sarea și sărurile de potasiu și magneziu din România*. Craiova, Romania: Intreprinderea poligrafica "Oltenia".

Talbot, C. J. (1998). Extrusions of Hormuz salt in Iran. *Geological Society, London, Special Publications*, 143, 315–334. https://doi.org/10.1144/GSL.SP.1998.143.01.21

Talbot, C. J., & Rogers, E. A. (1980). Seasonal Movements in a Salt Glacier in Iran. *Science*, 208, 395–397. https://doi.org/10.1126/science.208.4442.395

Tămaş, D. M., Schleder, Z., Krézsek, C., Man, S., & Filipescu, S. (2018). Understanding salt in orogenic settings: The evolution of ideas in the Romanian Carpathians. *AAPG Bulletin*, 102, 941–958. https://doi.org/10.1306/0913171615517088

Tămaş, D. M., Schleder, Z., Tămaş, A., Krézsek, C., Copoț, B., & Filipescu, S. (2019). Middle Miocene evolution and structural style of the Diapir Fold Zone, Eastern Carpathian Bend Zone, Romania: insights from scaled analogue modelling. In J. Hammerstein, R. Di Cuia, P. Griffiths, M. Cottam, G. Zamora, R. Butler (Eds.), *Fold and Thrust Belts: Structural Style, Evolution and Exploration* (Special Publications 490, pp. 267-284). Geological Society of London. https://doi.org/10.1144/SP490-2019-091

Ter Heege, J. H., De Bresser, J. H. P., & Spiers, C.J. (2005). Dynamic recrystallization of wet synthetic polycrystalline halite: dependence of grain size distribution on flow stress, temperature and strain. *Tectonophysics*, 396, 35–57. https://doi.org/10.1016/j.tecto.2004.10.002

Urai, J.L., Spiers, C.J., Zwart, H.J. and Lister, G.S. (1986). Weakening of Rock Salt by Water During Long-Term Creep. Nature 324: 554-557.

Urai, J. L., Schleder, Z., Spiers, C. J., & Kukla, P. A. (2008). Flow and Transport Properties of Salt Rocks. In R. Littke, U. Bayer, D. Gajewski, S. Nelskamp (Eds.), *Dynamics of Complex Intracontinental Basins: The Central European Basin System* (pp. 277-290). Springer-Verlag, Berlin. https://doi.org/10.1007/978-3-540-85085-4_5

Urai, J. L., Spiers, C. J., Peach, C. J., Franssen, R. C. M. W., & Liezenberg, J. L. (1987). Deformation mechanisms operating in naturally deformed halite rocks as deduced from microstructural investigations. *Geologie en Mijnbouw*, 66: 165-176.

Urecheatu, M. M., Tămaș, D. M., & Roban, R. D. (2019). *De la fotogrametrie 3D si modelare analogică la evoluția cinematică a diapirului de la Mânzălești*. Paper presented at National Geology and Geophysics Student Conference, Edition XX, Bucharest, Romania.

Voitești, I. P. (1943). *Sarea regiunilor carpatice Românești.* Bucharest, Romania: Fundația Regală pentru literatură și artă.

Weismüller, C., Urai, J. L., Kettermann, M., von Hagke, C., & Reicherter, K. (2019). Structure of massively dilatant faults in Iceland: lessons learned from high-resolution unmanned aerial vehicle data. *Solid Earth*, 10, 1757–1784. https://doi.org/10.5194/se-10-1757-2019

Willis, B. (1893). Mechanics of Appalachian structure. *U.S. Geological Survey Annual Report*, 13, part 2, 217-281.

Závada, P., Desbois, G., Urai, J. L., Schulmann, K., Rahmati, M., & Lexa, O. (2015). Impact of solid second phases on deformation mechanisms of naturally deformed salt rocks (Kuh-e-Namak, Dashti, Iran) and rheological stratification of the Hormuz Salt Formation. *Journal of Structural Geology*, 74, 117–144. https://doi.org/10.1016/j.jsg.2015.02.009

Zucker, E., Frumkin, A., Agnon, A., & Weinberger, R. (2019). Internal deformation and uplift-rate of salt walls detected by a displaced dissolution surface, Dead Sea basin. *Journal of Structural Geology*, 127, 103870. https://doi.org/10.1016/j.jsg.2019.103870

**FIGURES**

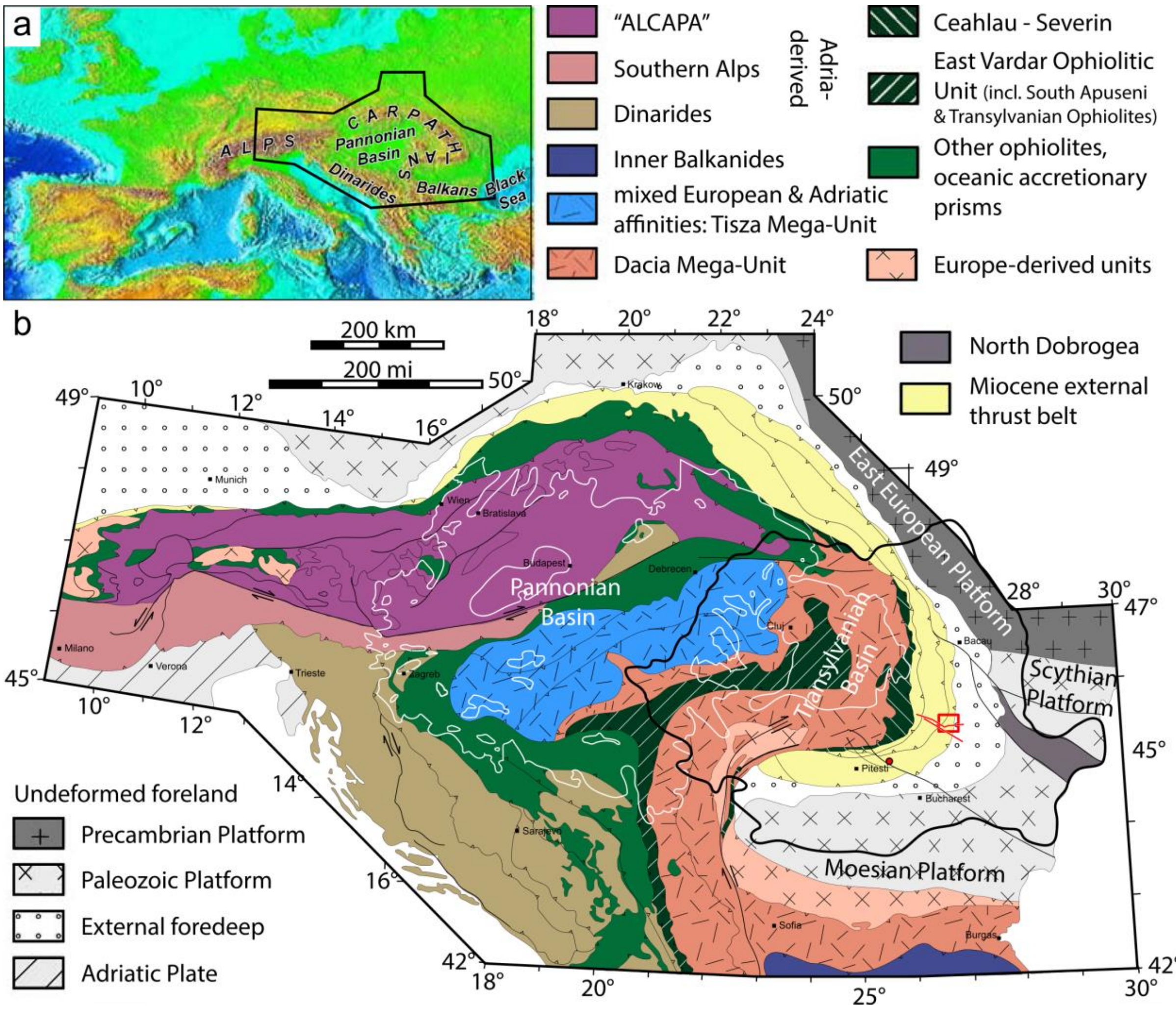


***Figure 1.***

Regional geological setting of the Romanian Carpathians. a) Topography of the Alpine–Dinaride–Carpathian system with solid black polygon indicating the location of (b) (after Merten et al., 2010). b) Simplified tectonic map of the Alps, Carpathians, and

Dinarides (after Schmid et al., 2008; Merten et al., 2010). ALCAPA = Alps, Carpathians, Pannonian unit. Red box is indicating the location of the geological map (Fig. 2a) and red lines are indicating the locations for the regional cross-sections (Figs. 2b, c). The red dot indicated the location of the small seismic line insert in figure 12a.

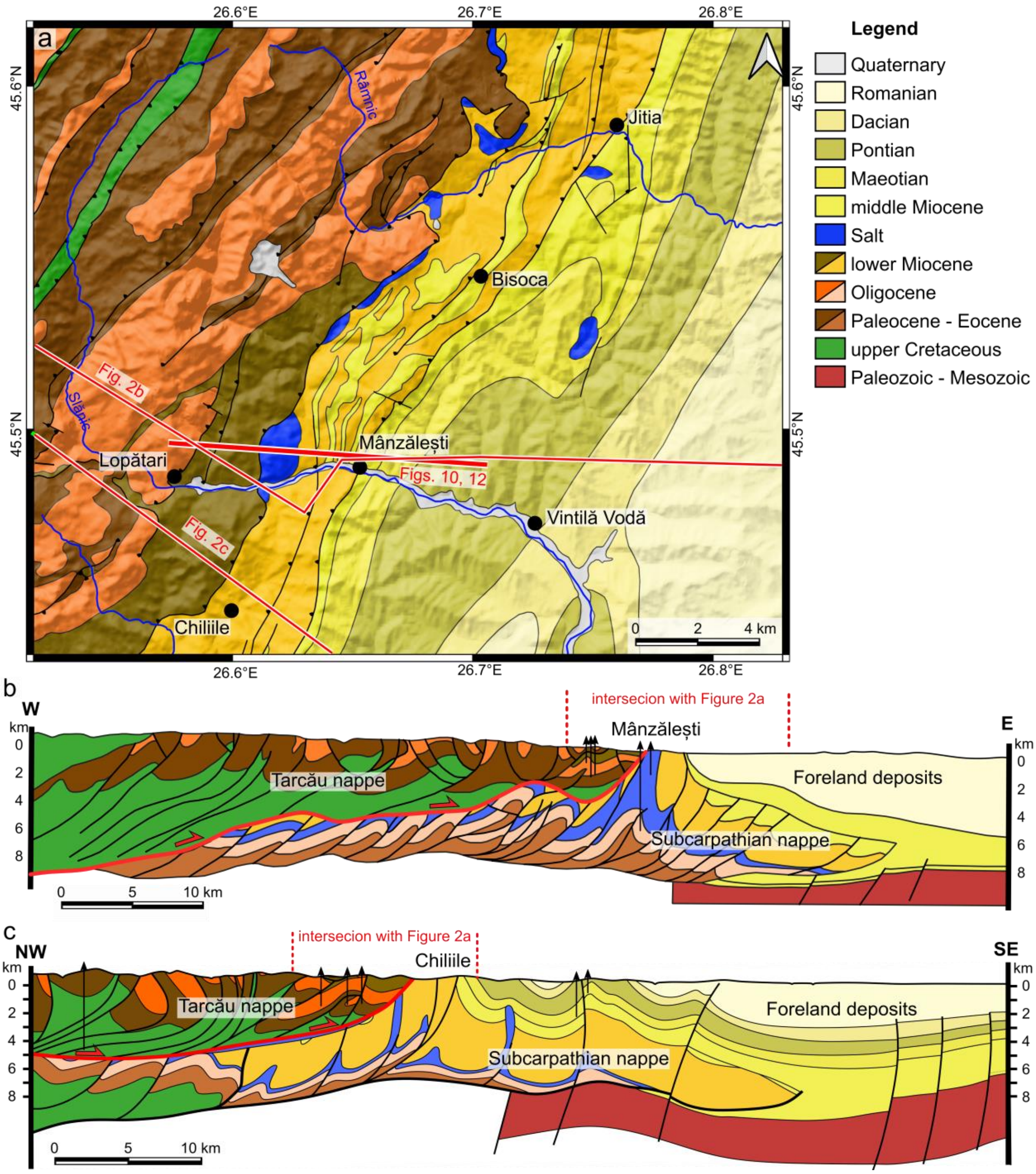


***Figure 2.***

(a) Surface geological map of the study area (Murgeanu et al., 1968) overlain on the EU-DEM v1.1 (grayscale hillshade). The sections in Figures 2b, c and 10 are marked with red lines on the map. (b) Regional geological profile through the southern part of the Eastern Carpathians, crossing the Mânzălești salt diapir, derived from surface geology and seismic sections (after Mațenco & Bertotti, 2000). (c) Regional geological profile through the southern part of the Eastern Carpathians, south of the Mânzălești salt diapir (after Ștefănescu et al. 1984).

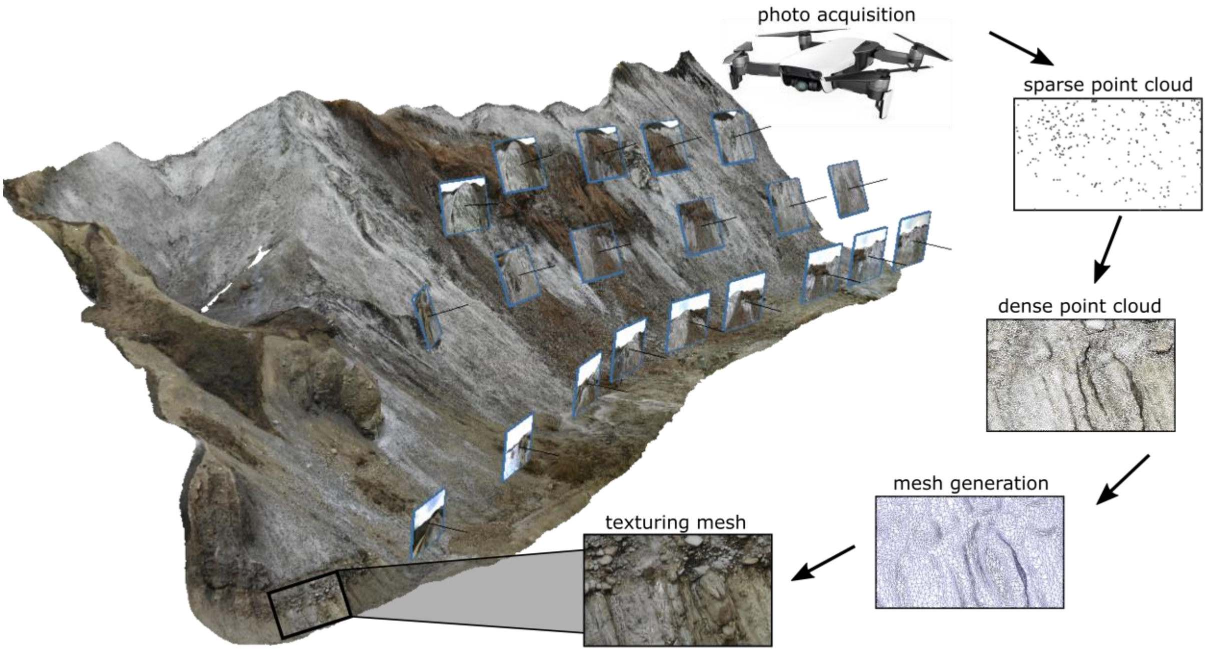


***Figure 3.***

Figure illustrating the main steps used in creating the digital outcrop models in Agisoft Metashape Professional (see Fig. 7 for more details on this DOM). Note that the photograph thumbnails in the figure are not the real number of images used to create this model.

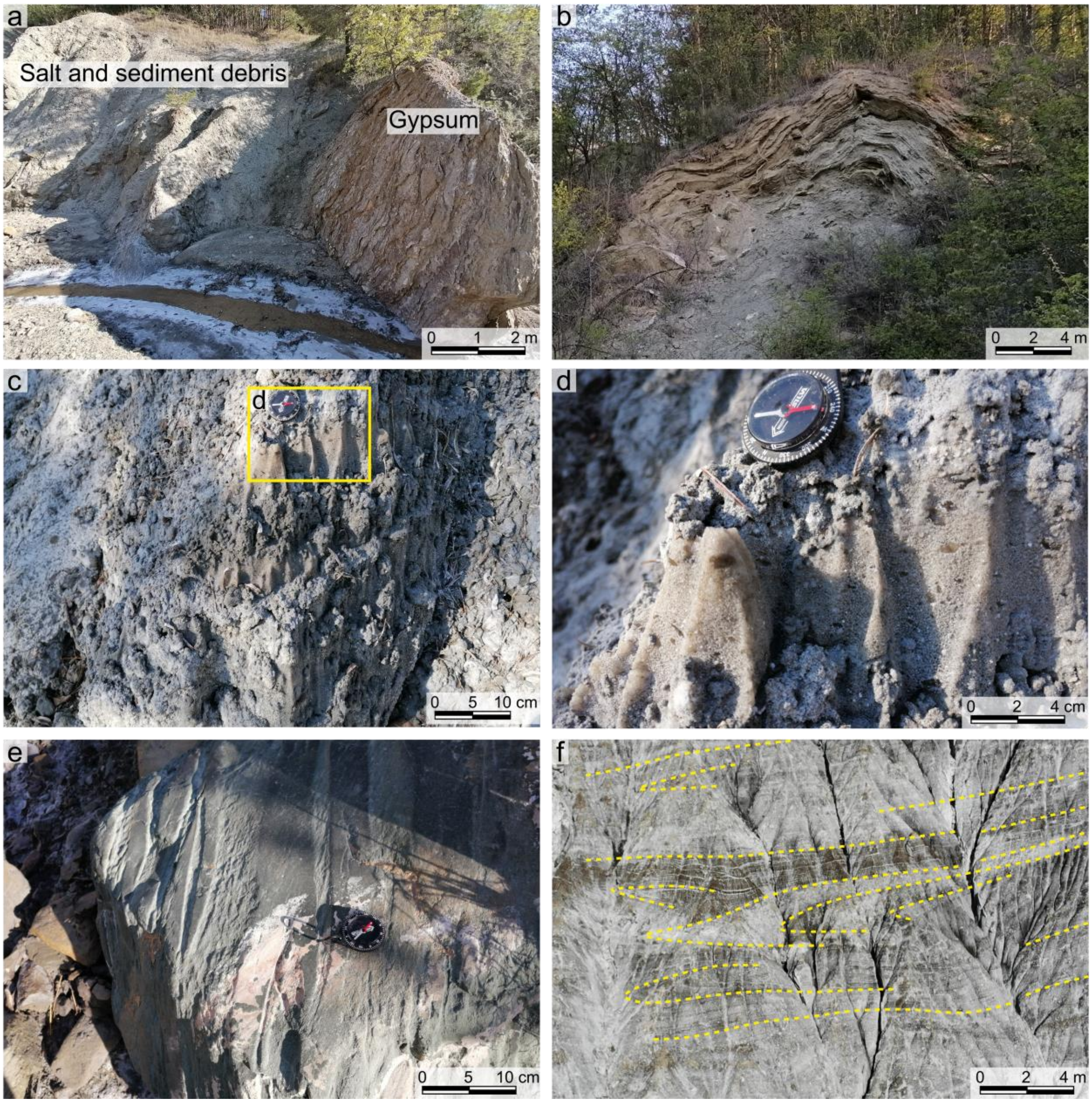


***Figure 4.***

Field photographs. (a, b) Folded gypsum layers on the northern flank of the diapir. (c, d) Salt exposure characterized by rillenkarren (solution grooves) – note the elongated and euhedral halite grains and large porphyroclasts. Most of the walls are covered by shale debris and recrystallised salt crusts. (e) Example of dm-scale exotic block – such cm- to m-scale clasts/blocks are found all along the valleys crossing the salt and on the steep outcrops, with the source for these from both the salt and the fluvial deposits on top of the salt diapir being eroded. (f) Drone close-up photograph of salt illustrating isoclinal folding. Figure locationis marked in Figs. 5, 8a.

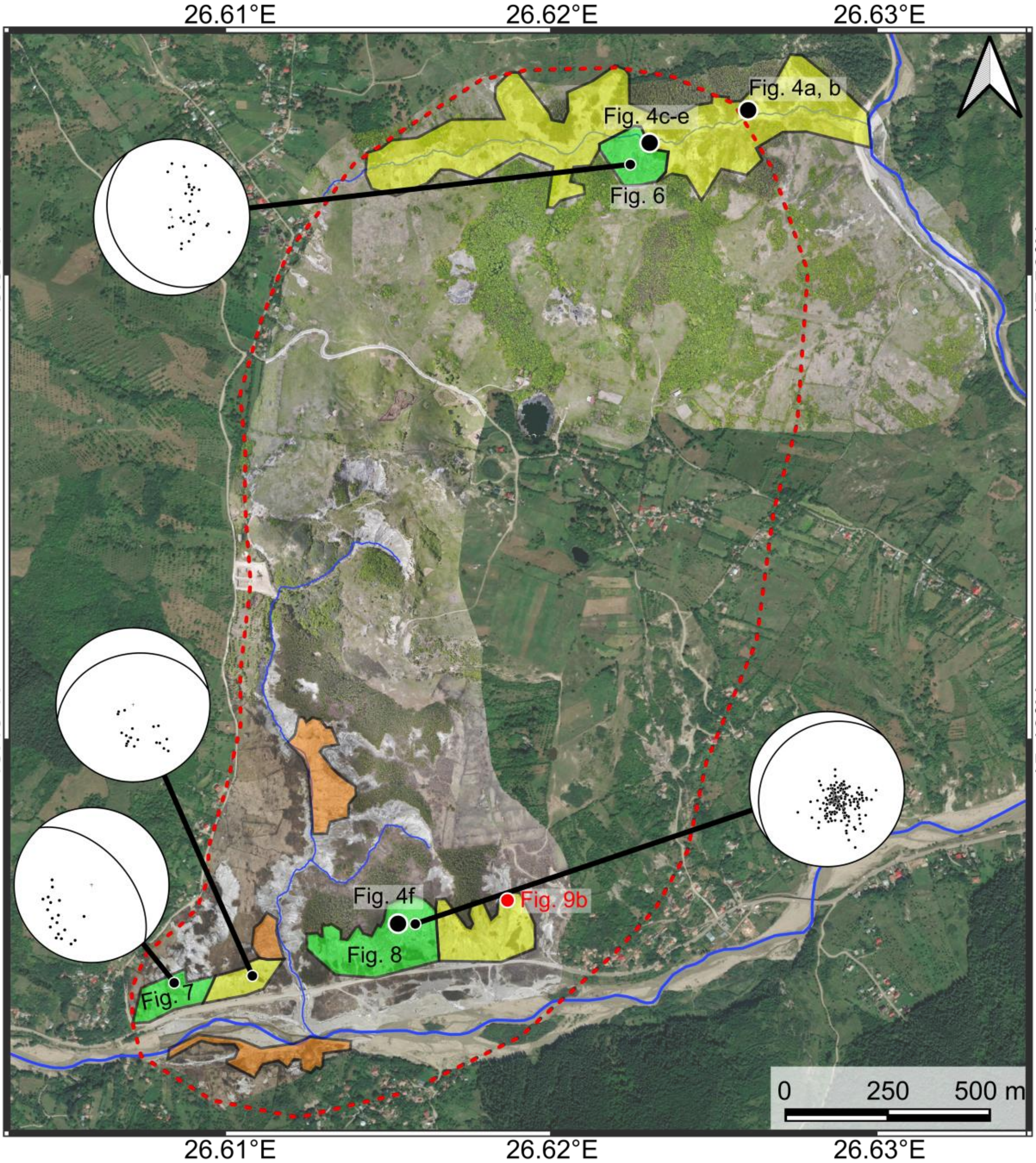


***Figure 5.***

Orthomosaic (light shading) overlaid on ESRI satellite image illustrating streams cutting the diapir (blue lines), the outline of the salt body (red dashed line), salt outcrops (white-light-grey outcrops), and the locations and exposure quality of the detailed DOM (Figs. 6-8). The models have been classified as good (green), moderate (yellow) or poor (orange) quality based on exposure, amount of debris cover and model-generation quality. Lower-hemisphere stereonet plots show poles to salt foliations and average orientations as great circles.

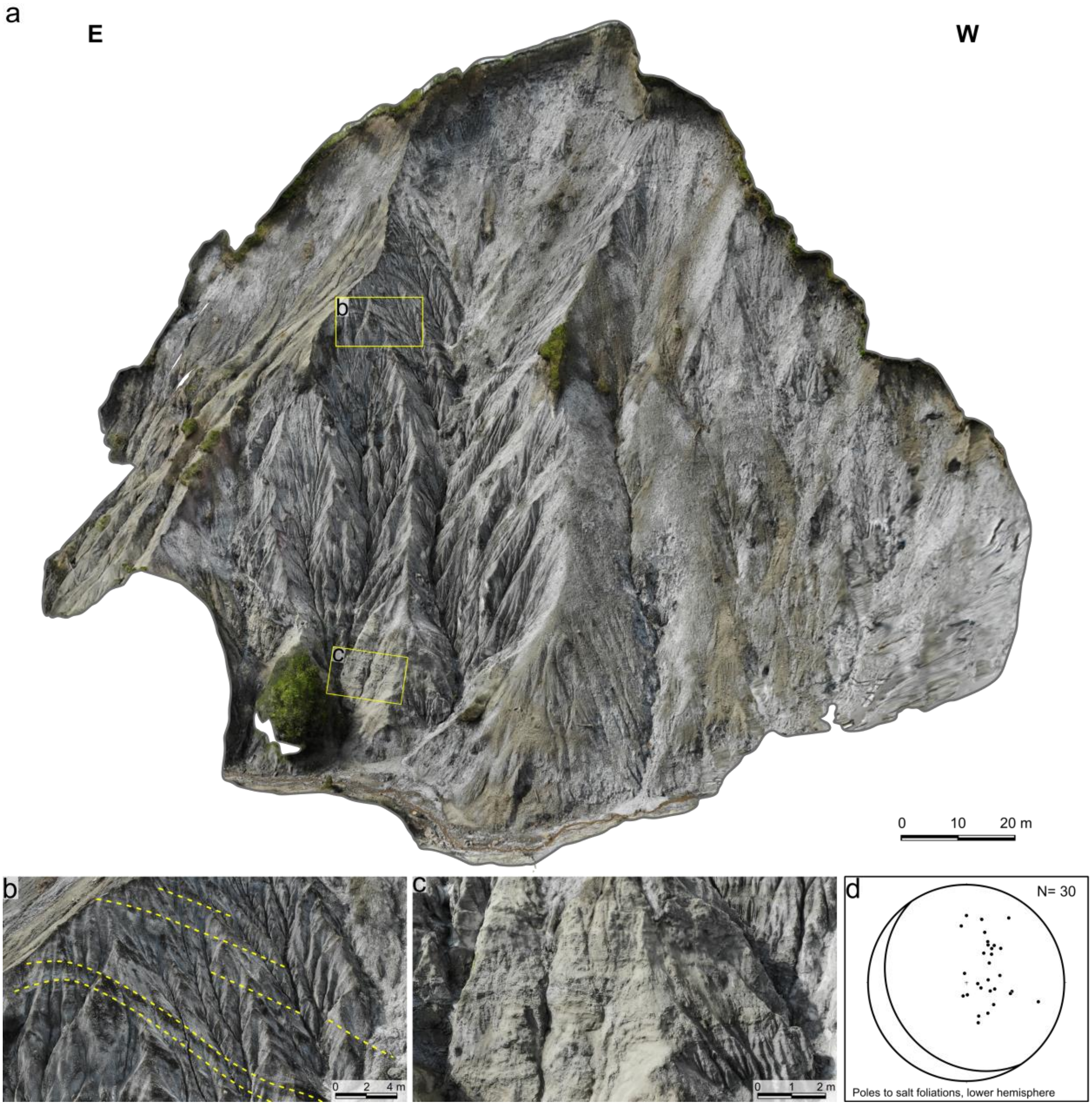


***Figure 6.***

(a) Sideview of DOM 1, located in the N of the Mânzălești salt diapir (with location of Figs. 6b, c). (b) Detailed image extracted from the DOM illustrating the salt foliation (marked with yellow dashed lines). (c) Detailed image extracted from the DOM illustrating salt interlayered with sandstones. (d) Lower-hemisphere stereonet plot showing poles to foliation and average orientation as a great circle.

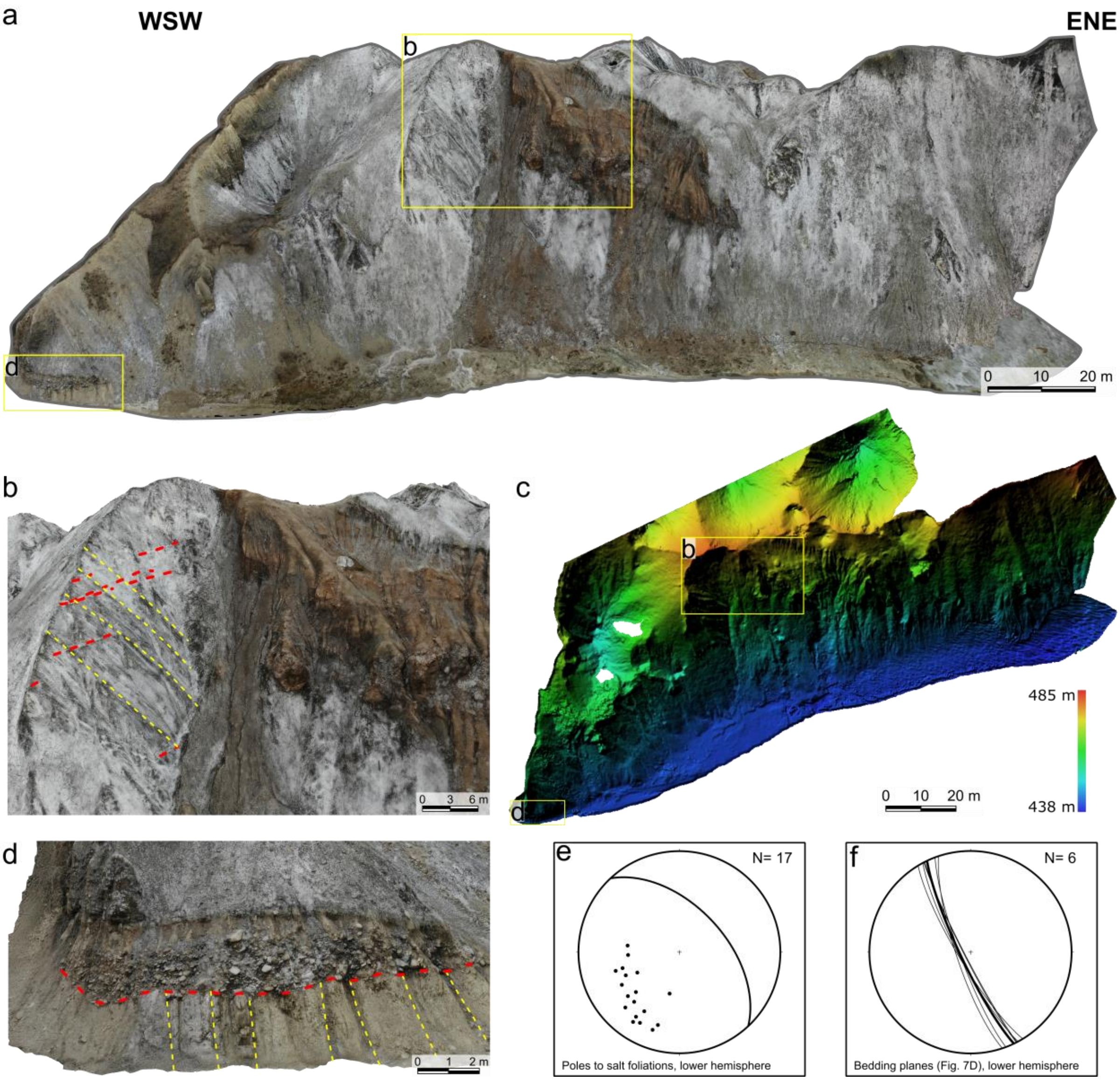


***Figure 7.***

(a) Sideview of DOM 2, located in the SW of the Mânzălești salt diapir (with location of Figs. 7b, c). (b) Detailed image extracted from the DOM illustrating the salt foliation (marked with yellow dashed lines; Fig. 7e) and the white bands cutting the foliation at a low angle (dashed red lines, see also Fig. 8a, b). (c) Digital elevation model (topview) illustrating a large number of sinkholes in the model and the location of Figs. 7b, d. (d) Detailed image extracted from the model illustrating the almost vertical bedding (dashed yellow lines) of the lower Miocene stratigraphy flanking the diapir and the discordant (dashed red line) nature of the Quaternary fluvial deposits and modern flow of salt on top of these. (e) Lower-hemisphere stereonet plot showing poles to salt foliation and average orientation as a great circle. (f) Lower-hemisphere stereonet plot showing the bedding planes of the near-vertical lower Miocene strata.

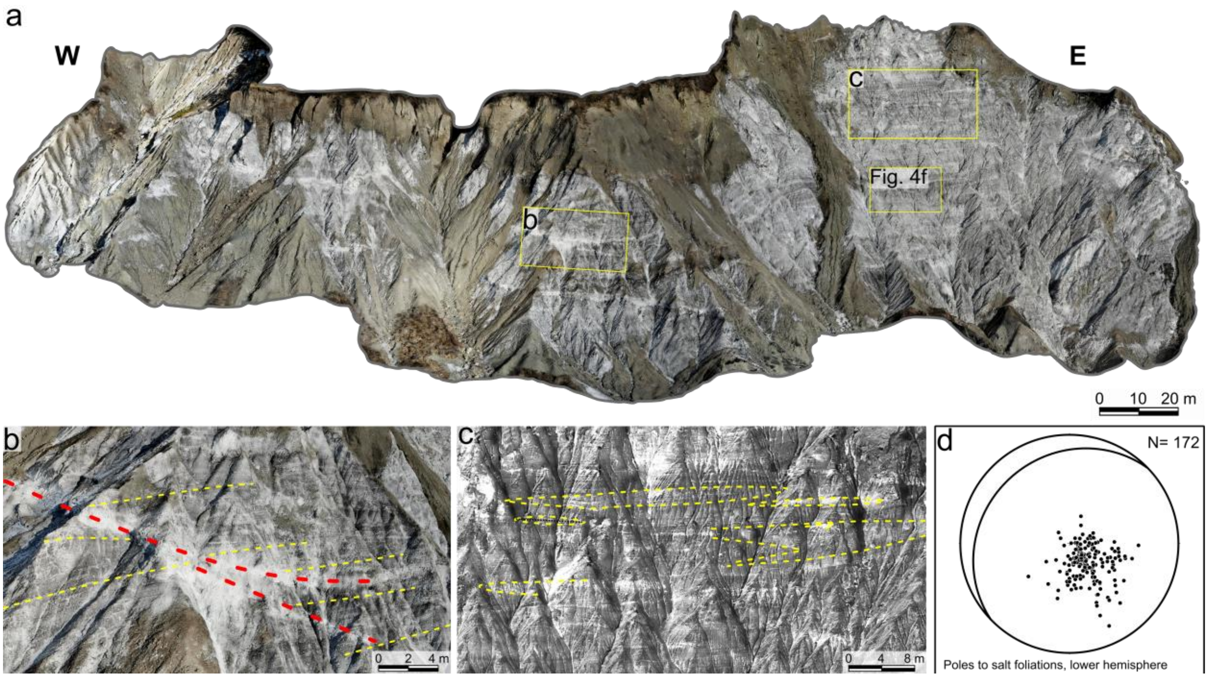


***Figure 8.***

(a) Sideview of DOM 3, located in the S of the Mânzălești salt diapir (with locations of Figs. 4d, 8b, c). (b) Detailed image extracted from the DOM illustrating the salt foliation (marked with yellow dashed lines; Fig. 8e) and the white bands cutting the foliation at a low angle (dashed red lines, see also Fig. 7b). (c) Detailed image extracted from the model illustrating isoclinal folding and tectonic lenses. (e) Lower-hemisphere stereonet plot showing poles to foliation (i.e. yellow dashed lines of Figs. 8b, c) and average orientation as a great circle.

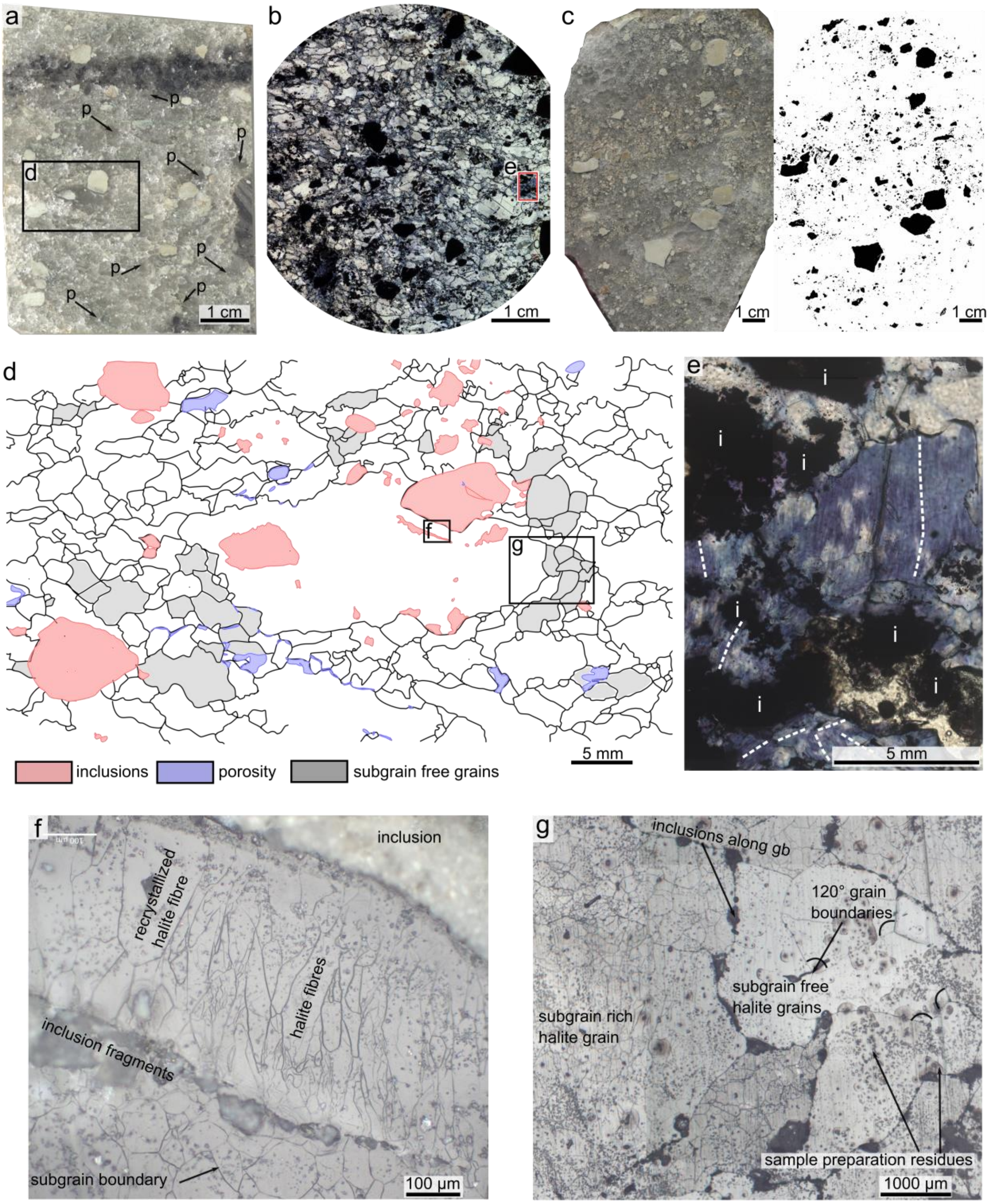


***Figure 9.***

(a) Thin-section photograph showing beige and black non-halite inclusions of variable grain sizes in a halite matrix with halite porphyroclasts *p* of up to 1 cm in diameter. (b) Micrograph of gamma-irradiated sample in ppl showing black non-halite inclusions and decorated blue halite. (c) Halite sample (left) showing distribution of particles (right) that was used for grainsize analysis. (d) Map of traced halite grain boundaries, inclusions, and pores from sample in Fig. 9a showing elongated and euhedral halite grains and large porphyroclast in the center; note inclusion fragments inside the porphyroclast. (e) Micrograph in ppl showing opaque inclusions *i* and blue striped gamma decoration in halite grains, indicated by strippled lines (location in Fig. 9b). (f) Reflected light micrograph showing halite fibres between fragmented non-halite inclusion (location in Fig. 9d). (g) Reflected light micrograph showing subgrains inside halite grain and subgrain-free halite grains with 120° grain boundaries and impurities along the boundaries (location in Fig. 9d). Small dark particles and brown halos (f, g) are due to etching residues on sample surface.

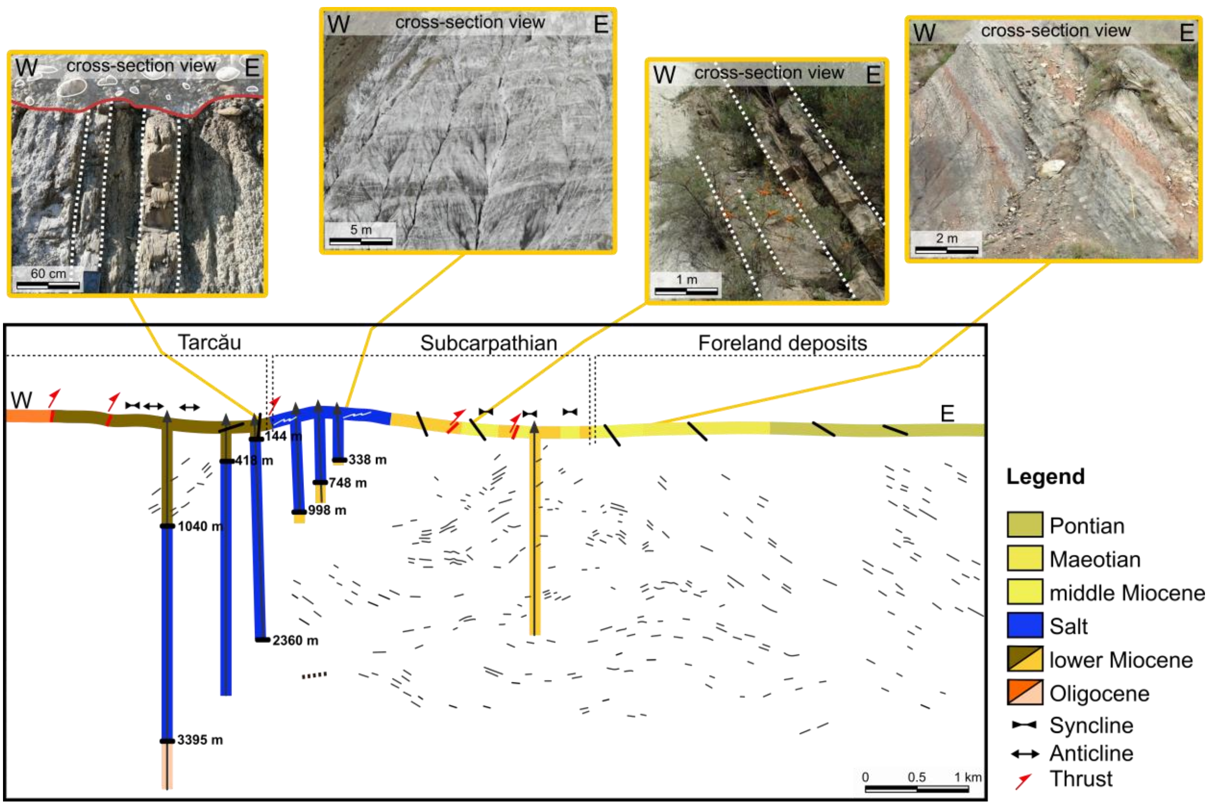


***Figure 10.***

Surface (Murgeanu et al., 1968) and subsurface well (Stoica & Gherasie, 1981; Marica, 2016) and seismic control on the cross-sectional geometry, with inset photos showing surface exposures. Thick black lines at the surface are measured bedding attitudes; thin black lines in the subsurface are tracings of seismic reflections. Wells are projected onto the line of section no more than 1 km. Location of cross section shown in Fig. 2a.

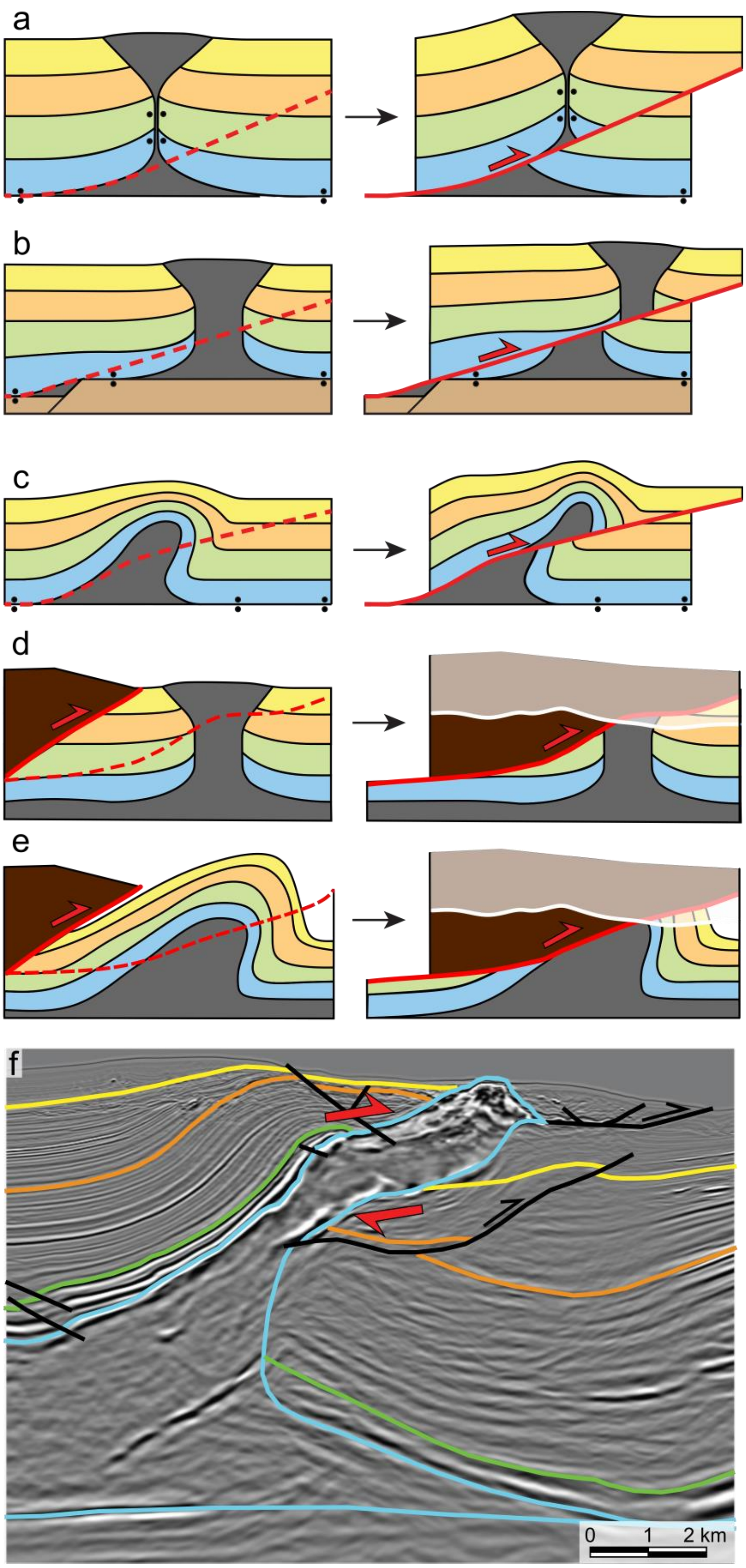


823

824 ***Figure 11.***

Salt-body decapitation. (a-e) Schematic diagrams showing different types of salt decapitation (salt in grey, pairs of dots indicate salt welds): (a) thrust fault emanating from pedestal after formation of vertical weld due to squeezing of diapir; (b) offset of diapir stem and squeezing of upper portion due to thrust fault ramping up from a basement step and intersecting a footwall diapir above pedestal; (c) salt-cored detachment fold modified by thrust fault, thereby becoming a decapitated diapir; (d) thrust nappe intersecting the upper part of a passive diapir; (e) salt-cored anticline decapitated by a thrust nappe. (f) Arbitrary line taken from 3-D depth-migrated seismic data from the Gulf of Mexico (where it is a combined divergent and convergent margin) showing salt diapir (blue) in the process of being decapitated during shortening (no vertical exaggeration, WesternGeco high-quality WAZ image).

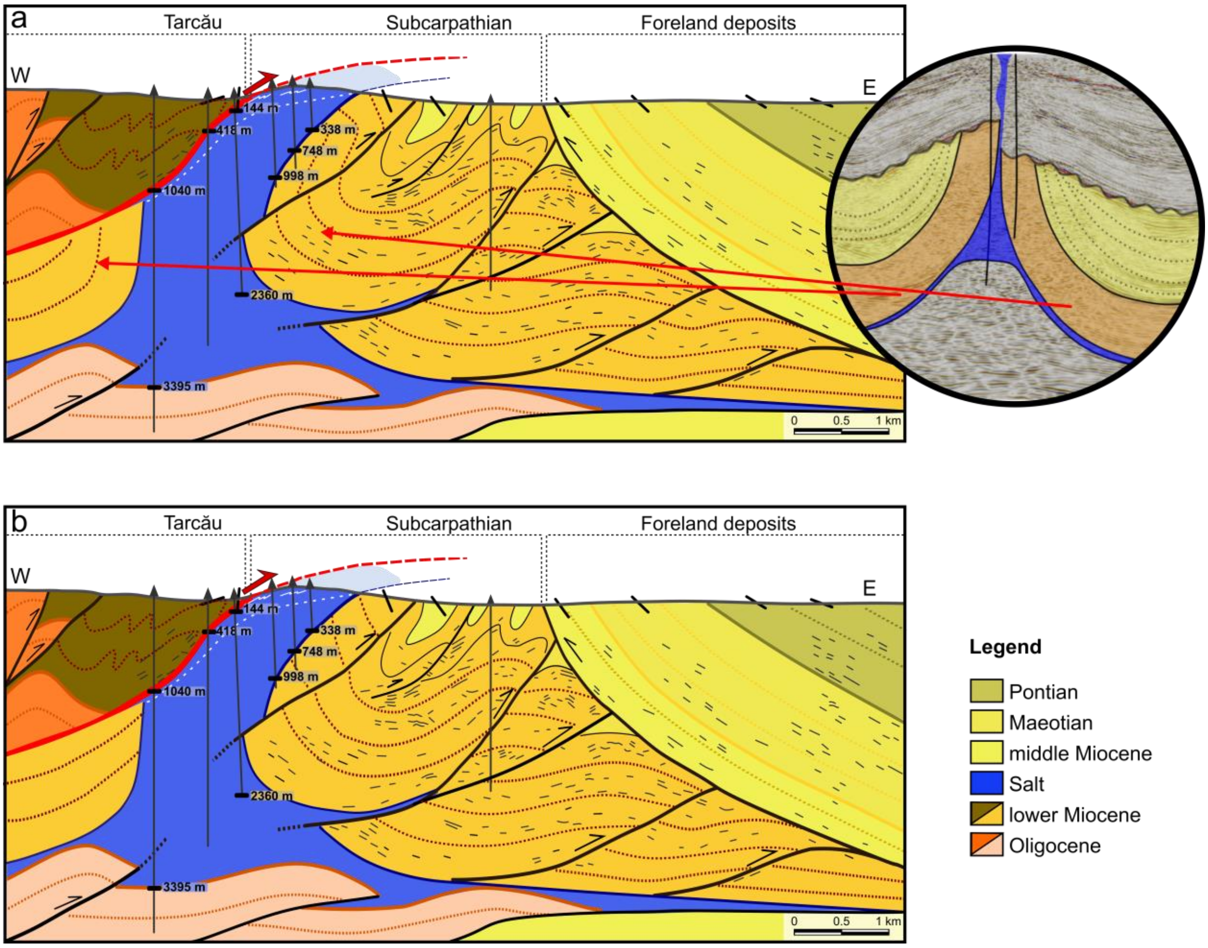


**Figure 12.**

Alternative cross-sections through the Mânzălești diapir based on the surface, seismic and well data shown in Fig. 10: (a) deep salt-cored anticline; (b) deep passive diapir. Sub-salt, the layers are most likely characterized by a duplex as suggested by Schleder et al. (2019) and Tămaș et al. (2019). Observations along strike (i.e. seismic insert in Fig 12a; Schleder et al., 2019) support the interpretation in (a).